



Cite this: *Phys. Chem. Chem. Phys.*, 2024, 26, 25557

# All-atom molecular dynamics simulations showing the dynamics of small organic molecules in water-solvated polyelectrolyte brush layers†

Leon A. Smook,<sup>a</sup> Raashiq Ishraaq,<sup>b</sup> Tanmay Sarkar Akash,<sup>b</sup> Sissi de Beer<sup>a</sup> and Siddhartha Das<sup>b</sup>

Polyelectrolyte brushes can introduce functionality to surfaces and because of this, these brushes have been studied extensively. In many applications, these brushes are used in solutions that contain a variety of molecules. While the interaction between polyelectrolyte brushes and molecules has been studied via coarse-grained simulations and experiments, such interaction has not been studied in molecular detail. An understanding of interactions in such molecular detail may prove crucial in the design of future brush coatings that can enable desired adsorption of different organic and biological molecules. Therefore, we present a first all-atom molecular dynamics simulations study of poly(sodium acrylate) brushes in contact with a small organic molecule,  $\gamma$ -butyrolactone. Within this molecular framework, we study the interaction of this lactone molecule with the brush layer and study the ensuing absorption and dynamics of the lactone inside the brush layer. The lactone is found to prefer to remain in the bulk solution; however, when absorbed, lactone molecules are found to have significantly reduced mobilities as compared to that in the bulk solution and are able to massively influence the properties of the brush-entrapped water molecules. These findings provide unprecedented details about the absorption-driven changes to molecular structure and dynamics of the lactone molecules and the water molecules inside the brush layer and can only be uncovered by our all-atom MD simulations. Such explicit and atomistically-resolved information, taking into account the specific chemical nature of the interacting systems, is rare in the context of designing polymer and PE brush-based coatings. Thus, we anticipate that our findings will be crucial in the design of future brush coatings aimed at providing adsorption platforms for different organic and biomolecules.

Received 23rd May 2024,  
Accepted 21st September 2024

DOI: 10.1039/d4cp02128b

rsc.li/pccp

## 1 Introduction

Polymer brushes are architectures where polymer chains are grafted onto a substrate with such high densities that interactions between neighboring chains make the chains deform from their unperturbed equilibrium configuration and stretch out in the form of ‘brushes’. These brushes are promising surface modifications since they resist bio-fouling<sup>1</sup> and create low-friction surfaces.<sup>2,3</sup> Due to these and other properties, the coatings created by grafting such polymer brushes to surfaces can be employed in a variety of applications. For instance,

polymer brushes have been used to enhance the efficiency of sponges to recover oil after spills;<sup>4</sup> to increase the selectivity of mixed-mode membranes;<sup>5</sup> to create wound-disinfecting nanotubes;<sup>6</sup> to functionalize nanoparticles that reduce dendrite formation in battery electrodes;<sup>7</sup> to functionalize nanoparticles that can increase the water transport through membranes;<sup>8</sup> to tune surface wettability;<sup>9,10</sup> or to create biosensing field-effect transistors.<sup>11</sup> Hence, these coatings find applications in fields ranging from separation technology to medicine and battery technology.

Polyelectrolyte (PE) brushes are a subclass of polymer brushes where the grafted chains are polyions.<sup>12,13</sup> Polyelectrolyte brushes by themselves have been theoretically researched extensively over the years using scaling theories and mean-field models,<sup>14–18</sup> self-consistent field calculations,<sup>19–21</sup> and coarse-grained molecular dynamics (MD) simulations.<sup>17,22–25</sup> These works provide a good picture of the physics of these polyelectrolyte brushes and describe the effects of grafting density, linear charge density, external salt concentration, and external stimuli

<sup>a</sup> Department of Molecules and Materials, MESA+ Institute, University of Twente, Enschede, The Netherlands. E-mail: l.a.smook@utwente.nl

<sup>b</sup> Department of Mechanical Engineering, University of Maryland, College Park, MD 20742, USA

† Electronic supplementary information (ESI) available: OPLS-AA force field parameters; brush height convergence; lactone absorption along trajectory; water structure of non-solvating water; water coordination number. See DOI: <https://doi.org/10.1039/d4cp02128b>



on these systems. Traditionally, research on polyelectrolyte brushes has been conducted from a polymer physics perspective considering generic interaction potentials. Such an approach, while it enables capturing very large polymeric systems, primarily considers a coarse-grained description of the PE system (thereby forbidding accounting for the influence of the individual polymer atoms) with additionally coarse-graining the effect of surrounding water. Under such circumstances, the influence of the individual polymer atoms as well as the behavior of brush-supported (or specifically, individual atoms of the polymer chain supported) water molecules and ions remain elusive. Identifying this significant gap, over the last years, there has been significant effort devoted in probing the behavior of polymer<sup>26–29</sup> and PE brushes using all-atom MD simulations. These simulations unravel hitherto unknown properties of brush-supported water molecules and ions (e.g. identifying the “water-in-salt”-like responses of screening counterions inside brush layer,<sup>30</sup> massive changes in the mobilities or counterions and water molecules inside the brush layer,<sup>31</sup> significant changes in the factors determining the water–water hydrogen bonding inside brush layer,<sup>32,33</sup> and many more). Therefore, such all-atom MD simulations provide excellent scope for studying the behavior of PE brushes, brush-supported water and ions, as well as PE-brush-other-moiety interactions in unprecedented details with exciting opportunities of several novel discoveries.

In this paper, we employ all-atom MD simulations to capture the absorption behavior of a small  $\gamma$ -butyrolactone molecule in water–solvated PE brushes. While the inclusion of small particles inside a polymer layer has been studied using theory and coarse-grained simulations<sup>34–40</sup> and atomistically in neutral or zwitterionic brushes,<sup>41–47</sup> to the best of our knowledge, this is the first study employing all-atom MD simulations for capturing the absorption behavior of a small organic molecule in a densely-grafted water-solvated PE brush layer. In these earlier studies, the investigated particles have sizes that tend to be large compared to the size of a chemical monomer in the polymer, making it difficult to directly translate results from these studies to experimental systems. The interaction between single molecules and polymer brushes has also been investigated experimentally *via* single-molecule tracking experiments.<sup>48</sup> Some of the single-molecule studies use dyes like Rhodamines<sup>49–51</sup> or carbocyanine dyes like DiIC18.<sup>52</sup> These dyes often have a specific molecular structure including delocalized electrons and in some cases even an explicit positive charge. Other studies use larger molecules such as P2VP polyelectrolyte chains (110 kDa),<sup>53</sup> dextran (10 kDa),<sup>54</sup> or fluorescently labeled dodecanoic acid.<sup>54</sup> These studies reveal that the diffusion of molecules in/on polymer brushes is slower than bulk diffusion, sometimes by 4 orders of magnitude. However, the observed effects cannot be decoupled from the molecular features of the used probes, so the molecules in these single-molecule tracking studies only provide limited insight into the interaction between polymer brushes and dissolved molecules. This is precisely why the ability to study the interactions of small molecules with PE brushes using an all-atom MD framework, as has been attempted in this study, becomes important.

To unravel the absorption behavior of small molecules in polyelectrolyte brushes, we study the interaction between a common water–solvated polyelectrolyte (in brush-like) configuration and a model solute in chemical detail will all-atom molecular dynamics simulations. Our model system consists of a poly(acrylic acid) derivative, namely poly(sodium acrylate) or PSA, which has been used as coating materials to enhance water flux<sup>55</sup> and modulate ion transport<sup>56</sup> in membrane materials, and  $\gamma$ -butyrolactone is a small flavor molecule in products as varied as beer and beans.<sup>57</sup> While the lactone molecules prefer the bulk solution over the brush environment, the lactone molecules that do absorb are found to have significantly reduced mobilities as compared to those in the bulk solution. Additionally, the molecules massively influence the properties of the brush-entrapped water molecules as functions of their (lactone molecules) position with respect to the brush-absorbed water molecules. Such explicit modeling of the adsorption by the PE brushes, where we account for the atomistic specifics of the adsorbing molecule and the brush layer, will be important to understand the adsorption process and the consequent effects on the brush layer (and water molecules solvating such brush layer) for several situations<sup>58–62</sup> where the brushes are used as preferred platforms for the adsorption of different organic and biomolecules.

## 2 Methods

We performed all-atom molecular dynamics (MD) simulations capturing the interaction (and subsequent absorption) of  $\gamma$ -butyrolactone molecules in water–solvated poly(sodium acrylate) PE brushes. The  $\gamma$ -butyrolactone molecules are introduced in water above the solvated brush layer. These molecules interact with the PE brush layer *via* diffusion and in the process some of these molecules get absorbed in the brush layer. These brushes are considered to have a degree of polymerization ( $N$ ) of 25; the use of such short chains is commonplace for studying the behavior of PE brushes and brush-supported systems using all-atom MD simulations.<sup>21,30,31,63,64</sup> The systems were simulated in a simulation box with periodic boundary conditions in the  $x$  and  $y$  directions and fixed boundary conditions in the  $z$  direction. The fixed boundary condition was enforced by using a wall of Lennard-Jones (LJ) particles (hexagonal closed packing arrangement, lattice constant 3.612 Å) with a purely repulsive potential. We studied systems with different grafting densities ( $0.3 \text{ nm}^{-2}$  and  $0.6 \text{ nm}^{-2}$ ) and at different temperatures (300 K and 355 K). Our simulations consider a grafting density of  $0.3 \text{ nm}^{-2}$  and  $0.6 \text{ nm}^{-2}$ . While such grafting densities are very high, grafting densities of around  $0.5 \text{ nm}^{-2}$  have been achieved experimentally for neutral PMMA brushes.<sup>65,66</sup> We simulated the brushes and lactones using the OPLS-AA force field<sup>67</sup> and water using the three-site SPC/E model.<sup>68</sup> The values of the force-field parameters were taken from the OPLS database.<sup>67</sup> The parameters for the sodium counterion were taken from Joung *et al.*<sup>69</sup> The specific values of the different simulation parameters used in this work have been summarized in the ESI† (see Section S1).



All non-bonded, non-electrostatic interactions were modeled using a combination of a truncated and shifted Lennard-Jones (LJ) potential with a cutoff of 13 Å. Interactions between dissimilar atom types have been modeled using geometrically mixed Lennard-Jones parameters (following Lorentz–Berthelot mixing rules in line with those used in Joung *et al.*<sup>69</sup>), except for interactions between the SPC/E water molecules and Na<sup>+</sup> ions. Non-bonded electrostatic interactions were modeled using a Coulomb potential. The long-range portion of this potential was calculated using the particle–particle/particle-mesh (PPPM) solver.<sup>70</sup> The bond-lengths and angles of the SPC/E water molecules were fixed using the SHAKE algorithm.<sup>71</sup>

The simulations were set up in a modular fashion. Fully-stretched poly(sodium acrylate) chains were placed in the simulation box using moltemplate<sup>72</sup> in a 6 × 6 square array. SPC/E water molecules were placed in the available space between these chains. Simultaneously, a bulk mixture of lactone and SPC/E water was prepared and partially equilibrated using enhanced Monte Carlo.<sup>73</sup> The lactone concentration of this initial solution was 1.0 M. These initial configurations were combined in one simulation box. This procedure resulted in the simulation systems summarized in Table 1. We remark that the samples with the lower grafting density have roughly twice the number of water and lactone molecules as the simulation box varies in size to accommodate the 6 × 6 array of chains. First, the density of the simulation box was equilibrated in an NP<sub>z</sub>T ensemble (*i.e.* the walls are free to move towards each other in the out-of-plane *z*-direction) at a temperature of 300 K and a pressure of 1 atmosphere using a Nosé–Hoover thermostat and barostat with time constants of 200 ps (thermostat) and 2000 ps (barostat).<sup>74,75</sup> Second, the volume was fixed at the equilibrium value and the simulation was continued in the NVT ensemble using a Langevin thermostat (time constant, 200 ps; temperature 300 K).<sup>76</sup> The equilibration of the system was tracked by monitoring the convergence in the brush height (ESI, † Section S2) and the number of adsorbed molecules in the brush. In other words, we identify that the system has equilibrated when the brush height and number of molecules no longer vary with time (see Section S3 in the ESI†). Also, from each simulation, we use the last 5 ns of the trajectory as the production run (*i.e.* to generate the results). The most efficient way for ascertaining whether a particular quantity (in this case, the brush height) has converged or not is to test the autocorrelation function of this quantity and quantify the autocorrelation decay time. If this decay time is significantly smaller than the total time for which the trajectory is probed, we can infer that the chosen quantity has converged. Accordingly, we have performed the autocorrelation analysis of the brush height

(for different cases studied) for the 5 ns trajectory (production run is for 5 ns) (please see Fig. S2 in the ESI† document). For all the cases studied, we find an autocorrelation decay time of 0.32 ns or smaller. This means that the 5 ns simulation window is more than an order of magnitude larger than the autocorrelation decay time, indicating sufficient sampling.

All simulations were run in LAMMPS.<sup>77,78</sup> The positions of all atoms were dumped every 2 ps. The position data was subsequently analyzed in Python using MDAnalysis package for importing the data.<sup>79,80</sup> Visualizations were performed with OVITO.<sup>81</sup>

## 3 Results and discussion

### 3.1 Poly(sodium acrylate) brush structure

Before studying the behavior of the  $\gamma$ -butyrolactone and water, we first characterize the structure of the water-solvated poly(sodium acrylate) brush. We study these polyelectrolyte brushes at two grafting densities (0.3 nm<sup>-2</sup> and 0.6 nm<sup>-2</sup>) and at two temperatures (300 K and 355 K) to see whether variations of the system conditions affect the brush configuration. For compactness, we refer to these samples using the following coding for grafting density (3–0.3 nm<sup>-2</sup>; 6–0.6 nm<sup>-2</sup>) and temperature (*R*/room temperature – 300 K; *H*/high temperature – 355 K). For instance, 3R refers to the brush with a grafting density of 0.3 nm<sup>-2</sup> at a temperature of 300 K. For reference, we present this coding in Table 1. For visual reference, we provide a snapshot of the 6R-sample in Fig. 1(a).

Polymer brushes are often characterized based on their height and monomer density profiles. Here, we define the brush height as the height below which 99% of the polymer resides. The polymer brush layers studied here have heights ranging from 39.0 Å (3H) to 44.8 Å (6R). In the summarized data in Table 2, we observe the following two trends: first, the brush height increases with the grafting density and second, the brush height decreases with increasing temperature. These trends are in line with observations in previous work.<sup>32,82</sup> The temperature effect can be explained from the standpoint of an entropic effect: as temperature increases the contribution of entropy to the free energy becomes more pronounced since this contribution scales with temperature. This entropic effect promotes the collapse of the stretched chains; therefore, at higher temperatures the brush becomes more collapsed and compact.

The brush height *H* increases with the grafting density. The grafting density is large enough to ensure that the brushes behave as non-linear osmotic brushes; accordingly, the brush height increases linearly (with an offset) with the grafting density. Following previous work<sup>30</sup> based on Ahrens *et al.*<sup>83</sup> and Nair,<sup>84</sup> we can therefore write:

$$H = nb \frac{f + \sigma_{\text{eff}}^2 \rho}{1 + f} \quad (1)$$

where *n* is the number of repeat units (here 25), *b* the length of a repeating unit (equal to two C–C bonds; 3.057 Å), *f* the charge fraction (here *f* = 1),  $\rho$  the grafting density, and  $\sigma_{\text{eff}}$  the effective monomer diameter. Here we take  $\sigma_{\text{eff}} = \sqrt{2}\sigma$ , where  $\sigma$  is the LJ-parameter for carbon atoms on the poly(sodium acrylate) chain

**Table 1** Coding scheme and properties of simulated brushes in this work

| Code | Grafting density (nm <sup>-2</sup> ) | Temperature (K) | # Water | # Lactone |
|------|--------------------------------------|-----------------|---------|-----------|
| 3R   | 0.3                                  | 300             | 41 859  | 432       |
| 3H   | 0.3                                  | 355             | 41 859  | 432       |
| 6R   | 0.6                                  | 300             | 20 541  | 234       |
| 6H   | 0.6                                  | 355             | 20 541  | 234       |



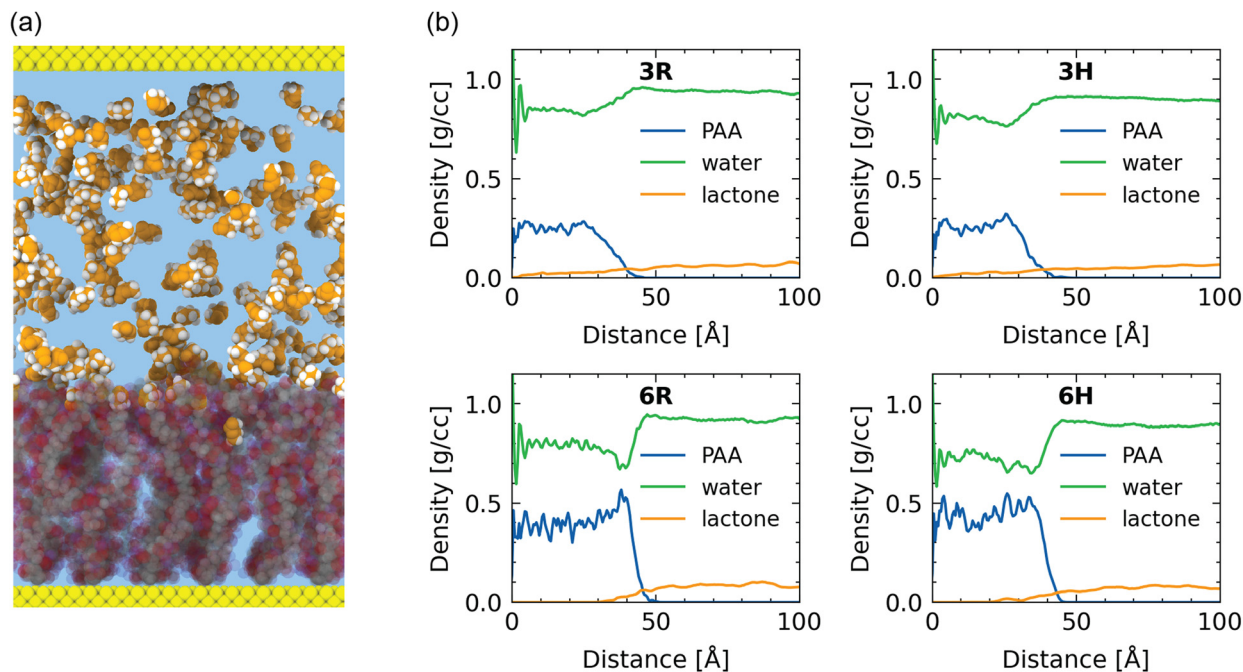


Fig. 1 (a) Visualized snapshot of  $\gamma$ -butyrolactone molecules in a poly(sodium acrylate) brush with  $\rho = 0.6 \text{ nm}^{-2}$  at  $T = 300 \text{ K}$ . Water molecules are not visualized for clarity. Brush (semitransparent) color legend: C (grey); O (red); H (white); Na (pink), wall (yellow). Lactone color legend: C/O (orange); H (white). (b) Density profiles of the systems studied.

Table 2 Summary of brush properties

|  | 3R                     | 3H                     | 6R                     | 6H                    |
|--|------------------------|------------------------|------------------------|-----------------------|
| Height [ $\text{\AA}$ ]                | 39.9                   | 39.0                   | 44.8                   | 42.1                  |
| $N_{\text{lact,brush}}$ [-]            | 81.6                   | 80.4                   | 13.2                   | 15.0                  |
| $N_{\text{wat,brush}}$ [-]             | 14 238                 | 13 180                 | 7230                   | 6211                  |
| $f_{\text{lact/wat,brush}}$ [-]        | $5.73 \times 10^{-3}$  | $6.10 \times 10^{-3}$  | $1.83 \times 10^{-3}$  | $2.42 \times 10^{-3}$ |
| $N_{\text{lact,bulk}}$ [-]             | 350.4                  | 351.6                  | 220.8                  | 219.0                 |
| $N_{\text{wat,bulk}}$ [-]              | 27 621                 | 28 679                 | 13 311                 | 14 330                |
| $f_{\text{lact/wat,bulk}}$ [-]         | $12.69 \times 10^{-3}$ | $12.26 \times 10^{-3}$ | $16.59 \times 10^{-3}$ | $15.2 \times 10^{-3}$ |
| $c$ [ $\text{nm}^{-3}$ ]               | 0.361                  | 0.361                  | 0.448                  | 0.425                 |
| $D$ [ $\text{\AA}^2 \text{ ps}^{-1}$ ] | 0.024                  | 0.050                  | 0.011                  | 0.025                 |

(3.5  $\text{\AA}$ ). These parameters give estimated brush heights of 41.0  $\text{\AA}$  for  $\rho = 0.3 \text{ nm}^{-2}$  (compare 39.9  $\text{\AA}$  – 3R; 39.0  $\text{\AA}$  – 3H) and 43.8  $\text{\AA}$  for  $\rho = 0.6 \text{ nm}^{-2}$  (compare 44.8  $\text{\AA}$  – 3R; 42.1  $\text{\AA}$  – 3H). Hence, we find good agreement between our observed values and the predicted values.

### 3.2 Absorption of $\gamma$ -butyrolactone molecules in the brush layer

Understanding and capturing the absorption of  $\gamma$ -butyrolactone molecules in the brush layer is the main topic of interest of this paper. We start with a setting where  $\gamma$ -butyrolactone molecules are present in the water layer that is present above the water-solvated brush layer. The  $\gamma$ -butyrolactone molecules interact with the brush layer *via* diffusion and in the process some amount of the  $\gamma$ -butyrolactone molecules get trapped inside the brush layer. This is the absorption phenomenon.

To quantify the absorption, we consider the ratio of lactone to water molecules inside the brush *versus* lactone to water molecules outside the brush. For the 3R case, the ratio of

lactone to water outside the brush is 12.69 lactone molecules per 1000 water molecules, while the same ratio reduces to only 5.73 molecules per 1000 water molecules inside the brush. For the 6R case, this ratio changes even more from 16.59 to 1.83  $\gamma$ -butyrolactone molecules per 1000 water molecules inside the brush.

This ratio reduction shows that the lactone molecules prefer more to stay outside the brush layer than inside the brush layer, which can readily be confirmed by looking at the density profiles in Fig. 1(b). As a consequence, the absorption is retarded but finite, as evident from the equilibrium values (per 1000 water molecules) of the number of lactone molecules present inside the brush layer. The size of the lactone molecules is much larger than the size of the water molecules: therefore, water will more easily penetrate into the densely grafted brush layer, as compared to the lactone molecules. This is a simple steric effect. This is even further evident for the more densely grafted brushes, justifying the progressive decrease in the number of lactone molecules (per 1000 water molecules) from the bulk to inside the brush layer with grafting density of  $0.3 \text{ nm}^{-2}$  and grafting density of  $0.6 \text{ nm}^{-2}$ .

We obtain some additional insight by observing the trajectories of the lactone molecules that have absorbed in the brush layer. Fig. 2 shows the trajectories of the  $z$ -coordinate of the absorbed lactone molecules that remain inside the brush for the complete duration of the production run (5 ns). These trajectories reveal that the lactones penetrate much more deeply into the sparser brushes that have a grafting density of  $0.3 \text{ nm}^{-2}$ , while they do not reach full depth in the denser brushes with a grafting density of  $0.6 \text{ nm}^{-2}$ . This observation



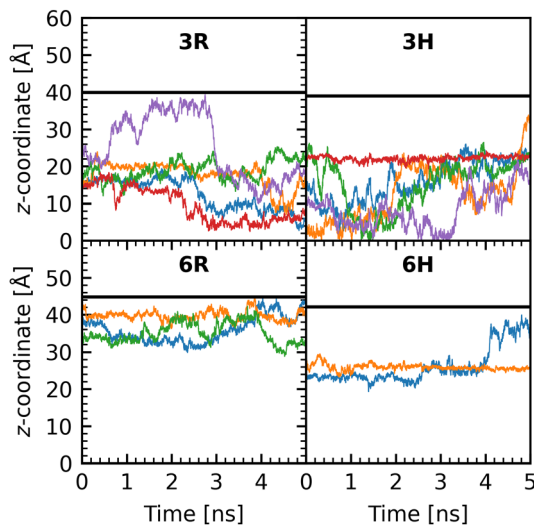


Fig. 2 Trajectories of lactone molecules in the polyelectrolyte brush. Each panel shows the height of the center-of-mass of a selection of up to 5 molecules that remain in the brush during the full production run (5 ns).

agrees with the absorption limitation as a result of the steric effects. Additionally, the trajectories reveal stationary periods (or periods of reduced mobilities), where the  $z$ -coordinate of the lactone remains rather constant. For instance, the lactone indicated with the red curve in 3H or the orange curve in 6H. These periods of reduced mobility characterize the lactone absorption in the PE brush layer.

### 3.3 Dynamics of $\gamma$ -butyrolactone molecules in the brush layer

One of the key features of all-atom molecular dynamics (MD) simulations is the ability to investigate systems in molecular detail. In our simulations, we can differentiate between  $\gamma$ -butyrolactone molecules that are in the solution *versus* those that are within the brush layer. To distinguish between  $\gamma$ -butyrolactone molecules inside and outside the brush, we identify the locations of the  $\gamma$ -butyrolactone molecules relative to the equilibrated brush height; all  $\gamma$ -butyrolactone molecules with atoms below this height are considered to be inside the brush.

To what extent do the dynamics of these molecules differ depending on their location in the system? In order to obtain the dynamics of these two types of the  $\gamma$ -butyrolactone molecules ( $\gamma$ -butyrolactone molecules inside the brush layer and  $\gamma$ -butyrolactone molecules outside the brush layer), we compute the mean squared displacements (MSDs) of the different types as a function of time and extract the corresponding diffusivities (see Fig. 3). The MSD-values of the lactones in the brush are lower than those in the bulk solution.

To obtain the diffusivity, we consider the MSD-*vs.*-time curve for lag times greater than 25 ps. For such times, the MSD-*vs.*-time curves are mostly linear and we obtain the diffusivity as  $D = \frac{1}{6} \frac{\partial}{\partial \tau} \text{MSD}(\tau)$ . As expected, the mean-squared displacements of the lactone molecules outside the brush layer depends only on temperature. At room temperature (300 K), the

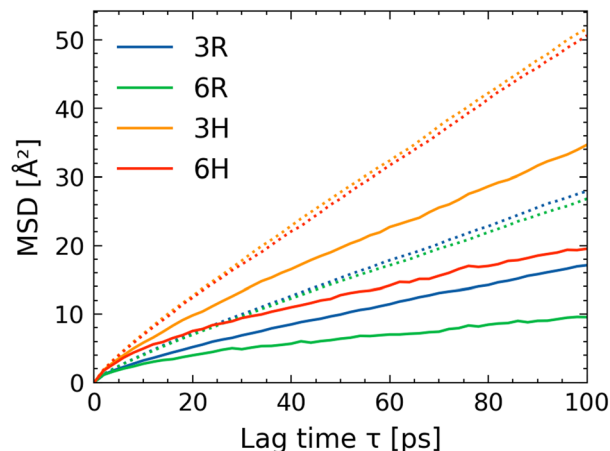


Fig. 3 Mean squared displacement (MSD) of lactone molecules in the four samples studied. Solid lines show the MSD for lactones inside the brush layer; dotted lines show the MSD for lactones outside the brush layer.

diffusivity of the lactone molecule in the bulk is  $0.041 \text{ \AA}^2 \text{ ps}^{-1}$  and at elevated temperature (355 K) it is  $0.080 \text{ \AA}^2 \text{ ps}^{-1}$ . The diffusivities are calculated in all cartesian directions and no significant differences between directions have been found at the time scales evaluated.

Inside the brush layer, however, the mobility of the lactone molecules is reduced. The diffusivity of the lactone decreases from  $0.041 \text{ \AA}^2 \text{ ps}^{-1}$  (bulk value) to  $0.024 \text{ \AA}^2 \text{ ps}^{-1}$  (3R) and to only  $0.011 \text{ \AA}^2 \text{ ps}^{-1}$  (6R). At elevated temperature, this effect is slightly less pronounced but the diffusivities still decrease from  $0.080 \text{ \AA}^2 \text{ ps}^{-1}$  (bulk value) to  $0.049 \text{ \AA}^2 \text{ ps}^{-1}$  (3H) and  $0.024 \text{ \AA}^2 \text{ ps}^{-1}$  (6H). Such reductions in diffusivities are not surprising. Interestingly, the directionality of the polymer seems to hardly affect the diffusivity of the lactone molecules; like for lactone molecules outside the brush, the diffusivity in all Cartesian directions is similar inside the brush. Previous all-atom simulations<sup>30,31</sup> have shown that the large confinement effect imparted by the brush layer leads to a significant reduction in the mobility of the brush-supported counterions and water molecules. Here, we establish that this confinement effect also leads to a significant decrease in the diffusivity of the brush-absorbed small organic molecules ( $\gamma$ -butyrolactone molecules); there is even experimental evidence of such reduced mobility of molecules absorbed in the brush layer.<sup>49–51,53,54</sup>

### 3.4 Behavior of the water molecules

The presence of the PE brushes affects not only the properties of the lactone molecules, but also the water molecules. In our previous papers employing all-atom MD simulations for probing the PE brushes, we have provided extensive results on the manner in which the presence of the brushes drastically alter the properties of the brush-supported water molecules. Here we shall discuss the manner in which the properties of such brush-supported water molecules get further affected by the additional presence of the brush-absorbed lactone molecules. For this purpose, we shall employ different measures to quantify



the water structure in the vicinity of the lactone molecules with the lactone molecules being either present in the bulk (outside the brush layer) or inside the brush layer. These measures include (1) orientation of water-dipoles around different parts of the lactone molecule (Fig. 4) and (2) the structural order of water molecules (around the lactone molecule) (Fig. 6).

**3.4.1 Water dipole distribution.** First, we probe the hydration shell around the lactone molecule. By looking at the dipole distribution of water molecules in the vicinity of different atoms of the lactone molecule, we can obtain an idea of the types of interactions that are at play. In the lactone molecule, we identify four different heavy atom types for which we compute this dipole distribution around these heavy atoms: these atoms (identified in bold) are (1) the oxygen in the carbonyl [**O**(=C)], (2) the carbon in the carbonyl [**C**(=O)], (3) the alkoxy oxygen [**O**(C)(C)], and (4) the aliphatic carbons [**C**(H)(H)]. We compare the water-dipole distributions around these different atoms of the lactone molecules with those lactone molecules being either inside or outside the brush layer.

The distribution of dipole angles is shown in Fig. 4. In these distributions, we observe contributions of two main modes: one peaks around  $\sim 75^\circ$  and the other one around  $120^\circ$  (see Fig. 5 for the corresponding visual representation). The former mode corresponds to situations where the water dipole lies flat on the surface of the atom (see Fig. 5(a)); the latter corresponds to the situation where the O-H vector of the water molecule points to the atom (see Fig. 5(b)). In other words, the first mode is more representative of the hydrophobic behavior (*i.e.* the water is interacting with a hydrophobic solute) and the second mode is more representative of hydrophilic behavior with

strong hydrogen bonds (*i.e.* the water is interacting with a hydrophilic solute). Furthermore, we find that the difference in water dipole distributions (around these four atoms) is not significant when comparing the cases of water hydrating the lactones inside *versus* outside the brush. At high temperatures (355 K), this difference is almost zero. At lower temperatures (300 K), however, this difference, which is mostly observed around the oxygen atoms, is weak but present. For water molecules around the lactone molecules in the solution (*i.e.* outside the brush layer), the mode centered around  $120^\circ$  is slightly more prevalent than the water molecules around the lactone molecules within the brush layer: this indicates that the lactones may be slightly less capable of forming hydrogen bonds with water when they enter the brush layer. However, this discrepancy is small and is therefore not expected to change the entropy of the lactone inside the brush significantly. In other words, the hydration shell of the lactone is mostly preserved upon absorption in the brush layer.

**3.4.2 Order parameters.** Another way to look at the effect of absorption on the solvent structure is through order parameters. As a result of its hydrogen bonding network, pristine water has a tetrahedral structure such that each water molecule has four equidistant, equally spaced nearest neighbors. In such a structure, any two nearest neighbors make an angle of  $109.5^\circ$  with the central atom. Hence, one can define a tetrahedral order parameter ( $q_4$ ) which is 1 when this structure is present in a perfect condition. This metric can be constructed such that it is 0 if one considers an ideal gas (or something that is locally completely disordered).<sup>85</sup> Fig. 6 shows the tetrahedral order parameter (probability density profiles corresponding to

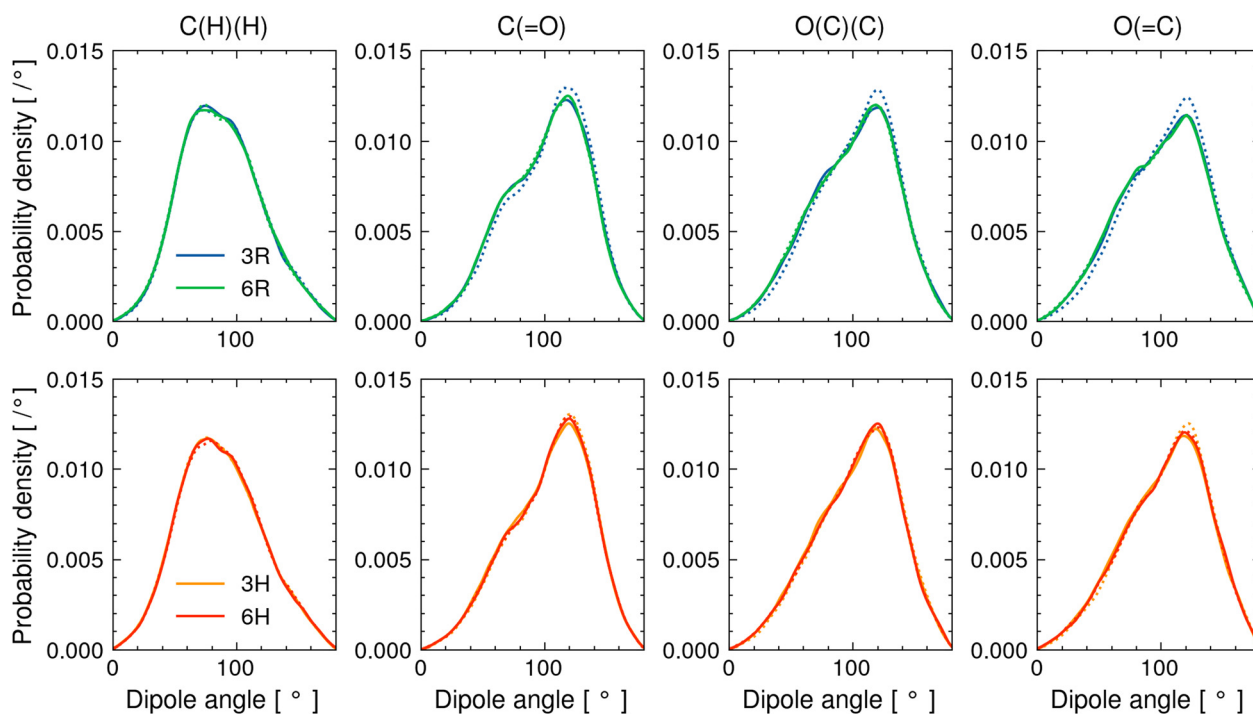


Fig. 4 Distribution of the angle of the water dipole of water atoms within 4 Å of different atoms in the lactone molecule. Solid lines indicate the distribution in the brush; dotted lines indicate the distribution in the bulk solution.



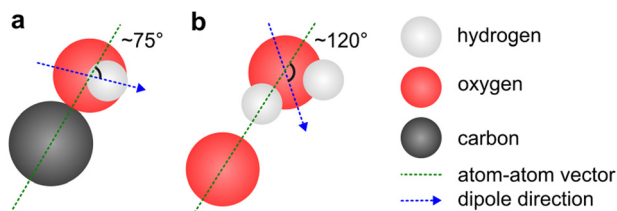


Fig. 5 Visual representation of different dipole angles around atoms. (a) Angle with a hydrophobic character. (b) Angle with a hydrophilic character and a hydrogen bond.

different values of the order parameter  $q_4$  have been plotted) for four different categories of water molecules: (1) water molecules outside the brush and at least 4 Å away from any lactone atom (of); (2) water molecules outside the brush and within 4 Å of any lactone atom (os); (3) water molecules inside the brush layer and at least 4 Å away from any lactone atom (if); (4) water molecules inside the brush and within 4 Å of any lactone atom (is). We point out that while the of-category is similar to bulk water, its structure is not identical to bulk water. At the bulk lactone concentrations on the order of 1 M, on the order of 1–2% of the molecules in solution are lactones. Hence almost all water molecules are in the vicinity of a lactone molecule, even if they are more than 4 Å away from the closest one. Nevertheless, the structure of the if and of water molecules in 6R samples with and without lactone were nearly identical (see Fig. S4, ESI<sup>†</sup>).

These probability density profiles (corresponding to different values of the order parameter  $q_4$ ) seem to have two peaks: one around  $q_4 \approx 0.78$  and another around  $q_4 \approx 0.46$ . These

peaks can be attributed to the regular tetrahedral order of water ( $\langle q_4 \rangle \approx 0.78$ ) and to tetrahedral order where a water molecule is located at an interstitial position ( $\langle q_4 \rangle \approx 0.46$ ).

Water inside the brush is always less structured than that in the bulk solution, stemming from the fact that the large confinement effect imparted by the PE brushes disrupts the water–water hydrogen bonding. For the case of 3R, we find that the structure of the free water (*i.e.*, water that is more than 4 Å away from the lactone molecule) is much less ordered inside the brush as compared to that outside the brush: hence, if we compare the cases of “if” and “of” for all the four cases (3R, 3H, 6R, and 6H), we find that that probability density profiles corresponding to the “of” show greater values of the peaks (as compared to the “if” cases) at  $q_4 \approx 0.78$  [see Fig. 6(a) and (d)]. The same dependence of the presence of the brush layer (in disrupting water structural order) is noted for the water molecules in close vicinity (within 4 Å) of the lactone molecules. Therefore, around the lactone molecules, the water structural order is more when the lactone molecules is outside the brush layer *versus* when the lactone molecules are inside the brush layer. This becomes obvious if one compares the cases of “os” and “is”: for all the four cases (3R, 3H, 6R, and 6H) we find that the probability density profiles corresponding to the “os” show greater values of the peaks (as compared to the “is” cases) at  $q_4 \approx 0.78$  [see Fig. 6(a) and (d)]. We note that water structure could also be affected by the coordination number, but the trends in this property are qualitatively different and cannot explain the changing water structure (see ESI<sup>†</sup>, Section S5). The lactone molecules do not affect the water structure in the brush (compare is and if), but they make the water less structured

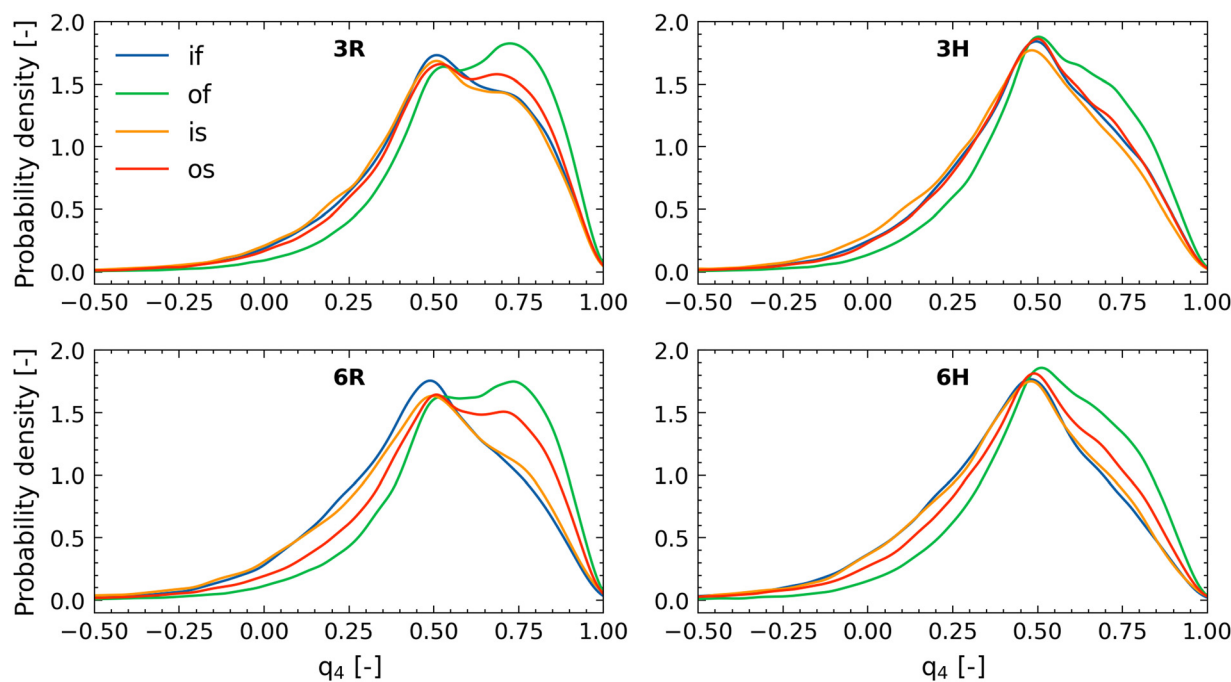


Fig. 6 Tetrahedral order parameters of different populations of water molecules in the system. if – inside the brush at least 4 Å from any lactone atom; is – inside the brush within 4 Å from any lactone atom; of – outside the brush at least 4 Å from any lactone atom; os – outside the brush within 4 Å from any lactone atom.



outside the brush (compare os and of), indicating that the lactone molecules have a slight chaotropic character.

## 4 Conclusions

In this work, we have employed all-atom MD simulation for studying the interactions between lactone molecules and poly(sodium acrylate) brushes and captured the subsequent absorption and mobility of the lactone molecules (within the brush layer) and the resulting changes in the properties of the brush-supported water molecules (in the vicinity of such brush-absorbed lactone molecules).

Using the capabilities of the all-atom MD simulations, we are able to point out the extent of absorption of the lactone molecules inside the brush layer. The numbers suggest that the lactone molecules prefer to remain in the bulk and have relatively weaker presence inside the brush layer. This can be primarily attributed to the significant steric effect imparted by the densely grafted brushes. However, even in the presence of such reduced number of absorbed lactone molecules, we are able to uncover highly intriguing dynamics of the lactone molecules inside the brush layer as well as interesting properties of the water molecules inside the brush layer as functions of their relative distances from the lactone molecules. For example, the diffusivities of the absorbed lactone molecules are reduced inside the brush layer, as compared to that in the bulk. This is in line with the ability of the brushes to significantly reduce the mobility of other entrained species (like water and ions). On the other hand, very interestingly, we find that while the dipole moments of water molecules show very weak variation as functions of their relative positions with respect to the lactone molecules (with the lactone molecules being either inside or outside the brushes), the water structural order parameter is significantly influenced depending on whether the corresponding lactone molecules are inside or outside the brushes (for all cases of grafting densities and temperatures, water molecules inside the brush layer have distinctly disrupted structural order as compared to water molecules outside the brush layer). We anticipate that this study will motivate several future studies that will employ all-atom MD simulations to better understand (with atomistically resolved information on water structure, structure of the polymers, and structure of interacting species) the absorption of a wide class of species on charged and uncharged polymer brush based coatings.

## Data availability

The data that support the findings of this study are openly available in the 4TU. Research Data database at <https://doi.org/10.4121/7b96bcc9-b5c1-4b47-a0b9-a970c3cb8972>.

## Conflicts of interest

There are no conflicts to declare.

## Acknowledgements

This publication is part of Targets 1 and 5 of the TTW Perspectief research programme ReCoVR: Recovery and Circularity of Valuable Resources which is (partly) financed by the Dutch Research Council (NWO). The authors acknowledge the support of the Deepthought2 High-Performance Computing cluster at the University of Maryland. NWO and SURFsara are acknowledged for HPC resources and support (project ref EINF-9565).

## Notes and references

- 1 Y. Higaki, M. Kobayashi, D. Murakami and A. Takahara, *Polym. J.*, 2016, **48**, 325–331.
- 2 C. Drummond, *Phys. Rev. Lett.*, 2012, **109**, 154302.
- 3 M. A. Abdelbar, J. P. Ewen, D. Dini and S. Angioletti-Uberti, *Biointerphases*, 2023, **18**, 010801.
- 4 Y. Liu, X. Wang and S. Feng, *Adv. Funct. Mater.*, 2019, **29**, 1902488.
- 5 H. Wang, S. He, X. Qin, C. Li and T. Li, *J. Am. Chem. Soc.*, 2018, **140**, 17203–17210.
- 6 Y. Yang, L. Ma, C. Cheng, Y. Deng, J. Huang, X. Fan, C. Nie, W. Zhao and C. Zhao, *Adv. Funct. Mater.*, 2018, **28**, 1705708.
- 7 S. Li, J. Huang, Y. Cui, S. Liu, Z. Chen, W. Huang, C. Li, R. Liu, R. Fu and D. Wu, *Nat. Nanotechnol.*, 2022, **17**, 613–621.
- 8 L. Dai, F. Xu, K. Huang, Y. Xia, Y. Wang, K. Qu, L. Xin, D. Zhang, Z. Xiong, Y. Wu, X. Guo, W. Jin and Z. Xu, *Angew. Chem., Int. Ed.*, 2021, **60**, 19933–19941.
- 9 V. S en echal, H. Saadaoui, J. Rodriguez-Hernandez and C. Drummond, *Langmuir*, 2017, **33**, 4996–5005.
- 10 V. Senechal, J. Rodriguez-Hernandez and C. Drummond, *Macromolecules*, 2022, **55**, 2636–2648.
- 11 S. Klinghammer, S. Rauch, S. Pregel, P. Uhlmann, L. Baraban and G. Cuniberti, *Micromachines*, 2020, **11**, 274.
- 12 S. Das, M. Banik, G. Chen, S. Sinha and R. Mukherjee, *Soft Matter*, 2015, **11**, 8550–8583.
- 13 M. Geoghegan, *Soft Matter*, 2022, **18**, 2500–2511.
- 14 R. S. Ross and P. Pincus, *Macromolecules*, 1992, **25**, 2177–2183.
- 15 P. Pincus, *Macromolecules*, 1991, **24**, 2912–2919.
- 16 T. Yamamoto and P. A. Pincus, *EPL*, 2011, **95**, 48003.
- 17 H. Merlitz, C. Li, C. Wu and J.-U. Sommer, *Soft Matter*, 2015, **11**, 5688–5696.
- 18 F. Csajka, R. Netz, C. Seidel and J.-F. Joanny, *Eur. Phys. J. E: Soft Matter Biol. Phys.*, 2001, **4**, 505–513.
- 19 C. Tong, *J. Chem. Phys.*, 2015, **143**, 054903.
- 20 B. M. Okrugin, R. P. Richter, F. A. M. Leermakers, I. M. Neelov, E. B. Zhulina and O. V. Borisov, *Polymers*, 2020, **12**, 898.
- 21 H. S. Sachar, V. S. Sivasankar and S. Das, *Soft Matter*, 2018, **15**, 559–574.
- 22 Y.-F. Ho, T. N. Shendruk, G. W. Slater and P.-Y. Hsiao, *Langmuir*, 2013, **29**, 2359–2370.



- 23 H. Ouyang, Z. Xia and J. Zhe, *Nanotechnology*, 2009, **20**, 195703.
- 24 S. Wang and C. Tong, *J. Appl. Phys.*, 2020, **127**, 074301.
- 25 F. Zhang, S. Wang, H. Ding and C. Tong, *Soft Matter*, 2019, **15**, 2560–2570.
- 26 D. E. S. Santos, D. Li, M. Ramstedt, J. E. Gautrot and T. A. Soares, *Langmuir*, 2019, **35**, 5037–5049.
- 27 U. R. Dahal, Z. Wang and E. E. Dormidontova, *Macromolecules*, 2017, **50**, 6722–6732.
- 28 G. Chen and E. Dormidontova, *Macromolecules*, 2022, **55**, 5222–5232.
- 29 G. Chen and E. E. Dormidontova, *Macromolecules*, 2024, **57**, 434–444.
- 30 H. S. Sachar, T. H. Pial, P. R. Desai, S. A. Etha, Y. Wang, P. W. Chung and S. Das, *Matter*, 2020, **2**, 1509–1521.
- 31 H. S. Sachar, T. H. Pial, B. S. Chava and S. Das, *Soft Matter*, 2020, **16**, 7808–7822.
- 32 H. S. Sachar, B. S. Chava, T. H. Pial and S. Das, *Macromolecules*, 2021, **54**, 6342–6354.
- 33 T. H. Pial and S. Das, *Soft Matter*, 2022, **18**, 8945–8951.
- 34 T. Curk, F. J. Martinez-Veracochea, D. Frenkel and J. Dobnikar, *Nano Lett.*, 2014, **14**, 2617–2622.
- 35 S. de Beer, L. I. S. Mensink and B. D. Kieviet, *Macromolecules*, 2016, **49**, 1070–1078.
- 36 V. Ermilov, A. Lazutin and A. Halperin, *Macromolecules*, 2010, **43**, 3511–3520.
- 37 J. Yaneva, D. Dimitrov, A. Milchev and K. Binder, *J. Colloid Interface Sci.*, 2009, **336**, 51–58.
- 38 J. Cheng, A. Vishnyakov and A. V. Neimark, *J. Chem. Phys.*, 2015, **142**, 034705.
- 39 H. Merlitz, C.-X. Wu and J.-U. Sommer, *Macromolecules*, 2012, **45**, 8494–8501.
- 40 L. A. Smook and S. de Beer, *ChemPhysChem*, 2023, **24**, e202300003.
- 41 M. Kanduč, W. K. Kim, R. Roa and J. Dzubiella, *Macromolecules*, 2018, **51**, 4853–4864.
- 42 M. Kanduč, R. Chudoba, K. Palczynski, W. K. Kim, R. Roa and J. Dzubiella, *Phys. Chem. Chem. Phys.*, 2017, **19**, 5906–5916.
- 43 T. Yagasaki and N. Matubayasi, *Langmuir*, 2023, **39**, 13158–13168.
- 44 T. Yagasaki and N. Matubayasi, *Phys. Chem. Chem. Phys.*, 2022, **24**, 22877–22888.
- 45 Y. Xiang, R.-G. Xu and Y. Leng, *Langmuir*, 2016, **32**, 4424–4433.
- 46 Y. Xiang, R.-G. Xu and Y. Leng, *Langmuir*, 2018, **34**, 2245–2257.
- 47 Y. Liu, D. Zhang, B. Ren, X. Gong, L. Xu, Z.-Q. Feng, Y. Chang, Y. He and J. Zheng, *J. Mater. Chem. B*, 2020, **8**, 3814–3828.
- 48 S. Wang, B. Jing and Y. Zhu, *J. Polym. Sci., Part B: Polym. Phys.*, 2014, **52**, 85–103.
- 49 C. Reznik, Q. Darugar, A. Wheat, T. Fulghum, R. C. Advincula and C. F. Landes, *J. Phys. Chem. B*, 2008, **112**, 10890–10897.
- 50 C. Reznik, N. Estillore, R. C. Advincula and C. F. Landes, *J. Phys. Chem. B*, 2009, **113**, 14611–14618.
- 51 L. C. C. Elliott, M. Barhoum, J. M. Harris and P. W. Bohn, *Langmuir*, 2011, **27**, 11037–11043.
- 52 L. C. C. Elliott, M. Barhoum, J. M. Harris and P. W. Bohn, *Phys. Chem. Chem. Phys.*, 2011, **13**, 4326–4334.
- 53 W. Wang, C. Zhang, S. Wang and J. Zhao, *Macromolecules*, 2007, **40**, 9564–9569.
- 54 H.-Y. Chin, D. Wang and D. K. Schwartz, *Macromolecules*, 2015, **48**, 4562–4571.
- 55 L. G. Lopez and R. J. Nap, *Phys. Chem. Chem. Phys.*, 2018, **20**, 16657–16665.
- 56 Y. Wang, L. Liu, J. Xue, J. Hou, L. Ding and H. Wang, *AIChE J.*, 2018, **64**(6), 2181–2188.
- 57 N. Garg, A. Sethupathy, R. Tuwani, R. NK, S. Dokania, A. Iyer, A. Gupta, S. Agrawal, N. Singh, S. Shukla, K. Kathuria, R. Badhwar, R. Kanji, A. Jain, A. Kaur, R. Nagpal and G. Bagler, *Nucleic Acids Res.*, 2017, **46**, D1210–D1216.
- 58 K. Ishihara, K. Mitera, Y. Inoue and K. Fukazawa, *Colloids Surf., B*, 2020, **194**, 111205.
- 59 C. Yoshikawa, S. Hattori, C.-F. Huang, H. Kobayashi and M. Tanaka, *J. Mater. Chem. B*, 2021, **9**, 5794–5804.
- 60 S. Sakata, Y. Inoue and K. Ishihara, *Langmuir*, 2015, **31**, 3108–3114.
- 61 H. Wang, H. Zhang, S. Yuan, C. Liu and Z. Xu, *J. Mol. Model.*, 2014, **20**, 2267.
- 62 M. Atif and A. Balasini, *Mater. Adv.*, 2024, **5**, 1420–1439.
- 63 T. H. Pial, H. S. Sachar, P. R. Desai and S. Das, *ACS Nano*, 2021, **15**, 6507–6516.
- 64 R. Ishraaq, T. S. Akash, A. Bera and S. Das, *J. Phys. Chem. B*, 2023, **128**(1), 381–392.
- 65 R. R. Patil, S. Turgman-Cohen, J. Šrogl, D. Kiserow and J. Genzer, *Langmuir*, 2015, **31**, 2372–2381.
- 66 Z. He, W. J. Xie, Z. Liu, G. Liu, Z. Wang, Y. Q. Gao and J. Wang, *Sci. Adv.*, 2016, **2**, e1600345.
- 67 W. L. Jorgensen, D. S. Maxwell and J. Tirado-Rives, *J. Am. Chem. Soc.*, 1996, **118**, 11225–11236.
- 68 H. J. C. Berendsen, J. R. Grigera and T. P. Straatsma, *J. Phys. Chem.*, 1987, **91**, 6269–6271.
- 69 I. S. Joung and T. E. Cheatham, *J. Phys. Chem. B*, 2008, **112**, 9020–9041.
- 70 R. W. Hockney and J. W. Eastwood, *Computer Simulations Using Particles*, McGraw-Hill, New York, 1989.
- 71 J.-P. Ryckaert, G. Ciccotti and H. J. Berendsen, *J. Comput. Phys.*, 1977, **23**, 327–341.
- 72 A. I. Jewett, D. Stelter, J. Lambert, S. M. Saladi, O. M. Roscioni, M. Ricci, L. Autin, M. Maritan, S. M. Bashusqeh, T. Keyes, R. T. Dame, J.-E. Shea, G. J. Jensen and D. S. Goodsell, *J. Mol. Biol.*, 2021, **433**, 166841.
- 73 P. J. in'T Veld and G. C. Rutledge, *Macromolecules*, 2003, **36**, 7358–7365.
- 74 S. Nosé, *J. Chem. Phys.*, 1984, **81**, 511–519.
- 75 W. G. Hoover, *Phys. Rev. A: At., Mol., Opt. Phys.*, 1985, **31**, 1695–1697.
- 76 T. Schneider and E. Stoll, *Phys. Rev. B: Solid State*, 1978, **17**, 1302–1322.
- 77 S. Plimpton, *J. Comput. Phys.*, 1995, **117**, 1–19.



- 78 A. P. Thompson, H. M. Aktulga, R. Berger, D. S. Bolintineanu, W. M. Brown, P. S. Crozier, P. J. in't Veld, A. Kohlmeyer, S. G. Moore, T. D. Nguyen, R. Shan, M. J. Stevens, J. Tranchida, C. Trott and S. J. Plimpton, *Comput. Phys. Commun.*, 2022, **271**, 108171.
- 79 N. Michaud-Agrawal, E. J. Denning, T. B. Woolf and O. Beckstein, *J. Comput. Chem.*, 2011, **32**, 2319–2327.
- 80 R. Gowers, M. Linke, J. Barnoud, T. Reddy, M. Melo, S. Seyler, J. Domański, D. Dotson, S. Buchoux, I. Kenney and O. Beckstein, *Python in Science Conference*, Austin, Texas, 2016, pp. 98–105.
- 81 A. Stukowski, *Modell. Simul. Mater. Sci. Eng.*, 2010, **18**, 015012.
- 82 A. E. Nasrabad, R. Laghaei and R. D. Coalson, *Int. J. Mol. Sci.*, 2023, **24**, 832.
- 83 H. Ahrens, S. Förster, C. A. Helm, N. A. Kumar, A. Naji, R. R. Netz and C. Seidel, *J. Phys. Chem. B*, 2004, **108**, 16870–16876.
- 84 A. Nair, PhD thesis, Universität Potsdam, 2006.
- 85 J. R. Errington and P. G. Debenedetti, *Nature*, 2001, **409**, 318–321.

